ANALYTICAL AND NUMERICAL ANALYSIS OF STAGING CONCEPTS IN ANNULAR GAS TURBINES

N. Noiray*, M. Bothien, B. Schuermans

Alstom Power – Brown Boveri Str., 5401 Baden, Switzerland
* Corresponding author: nicolas.noiray@power.alstom.com

In this work, the influence of azimuthal staging concepts on the thermoacoustic behavior of annular combustion chambers is assessed theoretically and numerically. Staging is a well-known and effective method to abate thermoacoustic pulsations in combustion chambers. However, in the case of for example fuel staging the associated inhomogeneity of equivalence ratio may result in increased levels of NO_x emissions. In order to minimize this unwanted effect a staging concept is desired in which the transfer function of the burners is altered while affecting the equivalence ratio as little as possible. In order to achieve this goal, a theoretical framework for predicting the influence of staging concepts on pulsations has been developed. Both linear and nonlinear analytical approaches are presented. A criterion based on the thermoacoustic coupling strength and on the asymmetry degree provides the modal behavior in the annular combustor, i.e. standing or traveling waves. The model predictions have been verified by numerical simulations of a heavy duty gas turbine using an in-house thermoacoustic network-modeling tool. The interaction between the heat release of the flame and the acoustic field was modeled using measured transfer functions and source terms. These numerical simulations confirmed the original theoretical considerations.

1 Introduction

Thermoacoustic coupling can lead to strong pressure oscillations in lean-premixed combustors. Many research teams work on thermoacoustic interactions in combustion systems especially with respect to the resulting pressure amplitudes which are governed by non-linear processes. This topic is also of utmost importance for the gas turbine industry since combustion instabilities can limit the operating regime of the engines or even cause structural damage [2,4,7]. In the particular case of annular combustion chambers, the interaction between flames and acoustics may amplify azimuthal acoustic modes of the combustor. These modes can be either spinning or standing. Practical observations show that both rotating [3, 10] and standing [3, 11] modes are common in the case of symmetric systems. However, if the conditions in gas turbines can really be said to yield a symmetric system is at least questionable. To gain further insight into these different observations the temporarily resolved ratio of standing and rotating part could be analyzed, a possible algorithm being proposed in Ref. [1]. These experimental observations have recently been reproduced by means of Large Eddy Simulation [12] or by using thermoacoustic network calculations [6, 9, 10]. Nevertheless the investigation of acoustic-flame and modal interactions on heavy-duty gas turbines are often limited because they are costly and the adequate instrumentation is difficult to implement. Furthermore, the mechanisms responsible for the dynamic nature of these azimuthal modes are not fully understood yet. In a recent interesting study, the influence of the system symmetry on the "standing/spinning" behavior is discussed [5]. This is done by investigating the properties of an annular Rijke tube model.
In the current paper, a third order saturation term is introduced into the equations describing the ther-

moacoustic coupling. The purpose is to derive simple relationships allowing to explain the nature of the modes as a function of different system parameters. This analysis differs from the one in Ref. [5] in which the phenomena are explained by making use of the group theory. Similar conclusions are drawn. A bifurcation parameter depending on acoustic source and loss strengths as well as on the source distribution determines the limit which defines whether a mode is standing or rotating. The theoretical work presented in Sec. 2 is compared to advanced thermoacoustic network calculations in Sec. 3. Section 4 deals with the influence of the distribution of dampers on their performance.

2 Theoretical model

2.1 Uniformly distributed transfer functions

First the non-dimensional wave equation with damping coefficient α and spatially distributed heat release rate Q is considered:

$$\nabla^2 p - \alpha \frac{\partial p}{\partial t} - \frac{\partial^2 p}{\partial t^2} = -\frac{\partial Q}{\partial t}. \tag{1}$$

where p and Q are the non-dimensional acoustic pressure and heat release rate. The pressure field can generally be expanded in series of orthogonal modes $p(\mathbf{x},t) = \sum_{n=1}^{\infty} \eta_n(t)\,\psi_n(\mathbf{x})$. A thin annular duct in which a thermoacoustic coupling operates is considered. It results from the combination of the eigenmodes sharing the n^{th} eigenvalue, which has the highest linear growth rate. The pressure field is then given by: $p(\theta,t) = \eta_1(t)\cos(n\theta) + \eta_2(t)\sin(n\theta)$ where θ is the azimuthal coordinate. Note that the subsequent analysis is completely analogous for annuli that are not thin and for cylinder modes (more generally for any rotational symmetric geometry).
The heat release is assumed to have a non-linear dependence of the pressure via a non-linear transfer function $Q = F(p)$. Note that if the heat release fluctuations do not depend directly on the pressure, but on acoustic velocity, then an impedance term should be introduced in the function F.
Substitution of the expression for the heat release and the pressure into eqn (1), multiplying both sides with $\cos(n\theta)$, integrating over θ ranging from 0 to 2π and making use of the orthogonality of the modes[1], yields the differential equation for η_1:

$$\ddot{\eta}_1 + \alpha\dot{\eta}_1 + n^2\eta_1 = \frac{1}{\pi}\int_0^{2\pi} \cos(n\theta)\frac{\partial F}{\partial t}\,d\theta. \tag{2}$$

A similar expression for η_2 is obtained by multiplying both sides with $\sin(\theta)$ before integrating:

$$\ddot{\eta}_2 + \alpha\dot{\eta}_2 + n^2\eta_2 = \frac{1}{\pi}\int_0^{2\pi} \sin(n\theta)\frac{\partial F}{\partial t}\,d\theta. \tag{3}$$

An approximate method will be used to solve the two equations: both modes η_1 and η_2 are assumed to be sinusoidal with fixed frequencies and amplitudes that vary only slowly in time: $\eta_1 = A(t)\sin(t)$ and $\eta_2 = B(t)\cos(t)$. Substituting this in the LHS of eqn (2), multiplying both sides with $\cos(t)$, integrating over time while taking into account the slowly varying function assumption yields:

$$\dot{A} + \frac{\alpha}{2}A = \frac{1}{2\pi}\int_0^{2\pi}\left(\frac{1}{\pi}\int_0^{2\pi}\cos(n\theta)\frac{\partial F}{\partial t}\,d\theta\right)\cos(t)\,dt. \tag{4}$$

A similar analysis applied to eqn (3) yields:

$$\dot{B} + \frac{\alpha}{2}B = -\frac{1}{2\pi}\int_0^{2\pi}\left(\frac{1}{\pi}\int_0^{2\pi}\sin(n\theta)\frac{\partial F}{\partial t}\,d\theta\right)\sin(t)\,dt. \tag{5}$$

[1] The orthogonal decomposition yields

$$\int_0^{2\pi}\cos(n\theta)\sin(n\theta)\,d\theta = 0 \quad \text{and} \quad \int_0^{2\pi}\cos^2(n\theta)\,d\theta = \int_0^{2\pi}\sin^2(n\theta)\,d\theta = \pi$$

The objective is now to expand the RHS of eqns (4) and (5) in order to obtain a differential system for the modal amplitudes A and B.
The non-linear function $Q = F(p)$ is assumed to fulfill the following conditions:

- it is a continuous, monotonically increasing function
- amplification is less than proportional (i.e. dF/dp is maximum for $p = 0$)
- the function is anti-symmetric: $F(-p) = -F(p)$

A Taylor expansion of such a function up to fourth order is then given as

$$F(p) = \beta\, p - k\, p^3, \quad \text{with} \quad \beta = \left.\frac{dF}{dp}\right|_{p=0} \quad \text{and} \quad k = -\frac{1}{6}\left.\frac{d^3F}{dp^3}\right|_{p=0}$$

where k and β are both positive. Note that the second and fourth order terms do not appear in the expansion due to the symmetry condition. The factor β can be considered as a linear coupling parameter between heat release and acoustic pressure (or linear frequency independent transfer function). The non-linear coupling between heat release and the acoustic field is represented by k.
Substituting the expression for F in the RHS of eqns (4) and (5), replacing p by $\eta_1\cos(n\theta) + \eta_2\sin(n\theta)$, integrating while considering that A and B are slowly varying functions yields the following system of equations for the modal amplitudes:

$$\dot{A} = \frac{1}{2}(\beta - \alpha)A - \frac{k}{32}(9A^2 + 3B^2)A \tag{6}$$

$$\dot{B} = \frac{1}{2}(\beta - \alpha)B - \frac{k}{32}(9B^2 + 3A^2)B \tag{7}$$

One can note that the derivation can be performed with heat release delayed response – which is observed in practical thermoacoustic systems – yielding the same type of coupled system for the modal amplitude interaction[2]. For the linear case, i.e. $k = 0$, the system stability is governed by the balance between the source and damping parameters α and β. The system is linearly stable if $\alpha > \beta$, thus if damping is stronger than driving by the heat release. On the other hand, perturbations will be exponentially amplified at a rate $(\beta - \alpha)$ if $\alpha < \beta$. However, it is not possible to conclude anything regarding the modal interactions since these two modes, which share the same degenerate eigenvalue are described with independent equations.
Accounting for the third order nonlinearity, the spinning nature of the limit cycle is now investigated. The fixed points of this system can be found by setting $\dot{A} = \dot{B} = 0$ in eqns (6) and (7), and solving for A and B, which yields four types of solutions:

$$\begin{array}{lll} \text{(solution 1)} & A = 0, & B = 0 \\ \text{(solution 2)} & A = \frac{4}{3}\sqrt{\frac{\beta-\alpha}{k}}, & B = 0 \\ \text{(solution 3)} & A = 0, & B = \frac{4}{3}\sqrt{\frac{\beta-\alpha}{k}} \\ \text{(solution 4)} & A = 2\sqrt{\frac{\beta-\alpha}{3k}}, & B = 2\sqrt{\frac{\beta-\alpha}{3k}} \end{array} \tag{8}$$

[2] Considering $F(p) = \beta p(t-\tau) - kp^3$. The integral associated with the linear contribution in the RHS of eqn (4) would then be

$$\frac{\beta}{\pi}\int_0^{2\pi}\cos(n\theta)\frac{\partial\big(p(t-\tau)\big)}{\partial t}d\theta = \beta\big(\dot{A}\sin(t-\tau) + A\cos(t-\tau)\big)$$

Eqn (6) is now written

$$\dot{A}\left(1 + \frac{\beta\sin(\tau)}{2}\right) = \frac{1}{2}(\beta\cos(\tau) - \alpha)A - \frac{k}{32}(9A^2 + 3B^2)A,$$

and since the source term is weak in real applications ($\beta \ll 1$), one obtains

$$\dot{A} = \frac{1}{2}(\beta\cos(\tau) - \alpha)A - \frac{k}{32}(9A^2 + 3B^2)A,$$

where we have $\beta\cos(\tau)$ instead of β in eqn (6). The delay is now defining whether the coupling between pressure and heat release rate acts as a source ($\cos(\tau) > 0$) or as an additionnal damping if it is negative.

Note that there are actually nine solutions, but the remaining solutions, are mirrored versions of the ones above. In order to analyze the stability of these solutions, eqns (6) and (7) are linearised around $\bar{A}$ and $\bar{B}$. The resulting system of equations represents the linear dynamics in a neighborhood of $(\bar{A},\bar{B})$:

$$\frac{d}{dt}\begin{bmatrix} A' \\ B' \end{bmatrix} = \begin{bmatrix} \frac{1}{2}(\beta-\alpha) - \frac{27}{32}\bar{A}^2 k - \frac{3}{32}k\bar{B}^2 & -\frac{3}{16}k\bar{B}\bar{A} \\ -\frac{3}{16}k\bar{B}\bar{A} & \frac{1}{2}(\beta-\alpha) - \frac{27}{32}k\bar{B}^2 - \frac{3}{32}\bar{A}^2 k \end{bmatrix}\begin{bmatrix} A' \\ B' \end{bmatrix}, \tag{9}$$

where $A' = A-\bar{A}$ and $B' = B-\bar{B}$. The eigenvalues of this system are real and characterize the nature of the fixed points given in (8): negative eigenvalues are stable, positive eigenvalues are unstable. Substituting the solutions of eqns (6) and (7) for $\bar{A}$ and $\bar{B}$ into eqn (9), and evaluating the matrix eigenvalues yields:

$$\begin{array}{lllll} \text{(solution 1)} & \lambda_1 = \frac{1}{2}(\beta-\alpha), & \lambda_2 = \frac{1}{2}(\beta-\alpha) & \rightarrow & \text{Repeller} \\ \text{(solution 2,3)} & \lambda_1 = \frac{1}{3}(\beta-\alpha), & \lambda_2 = (\alpha-\beta) & \rightarrow & \text{Saddlepoints} \\ \text{(solution 4)} & \lambda_1 = \alpha-\beta, & \lambda_2 = \frac{1}{2}(\alpha-\beta) & \rightarrow & \text{Attractor} \end{array} \tag{10}$$

Considering only cases where the linearised system would be unstable ($\beta > \alpha$), solution 1 has two unstable eigenvalues: it is a repeller. Solution 2 and 3 both have one stable and one unstable eigenvalue. Hence, these fixed points are saddle points and thus unstable. Solution 4 has two stable eigenvalues and is thus an attractor. It is the only stable solution, where both modes have equal amplitudes. The space-time dependence of the pressure of this solution is given by:

$$p(t,\theta) \quad = \quad 2\sqrt{\frac{\beta-\alpha}{3k}}\big(\sin(t)\cos(n\theta)+\cos(t)\sin(n\theta)\big) = 2\sqrt{\frac{\beta-\alpha}{3k}}\sin(t+n\theta), \tag{11}$$

which is a rotating mode. The analysis presented here shows that, in case of spatially uniform coupling between heat release rate and pressure, a linearly unstable azimuthal mode (in a uniform annular or cylindrical system) will always result in a traveling (rotating) wave for the given type of non-linearity (which is not very restrictive).

2.2 Non-uniform distribution of the transfer functions

It is now interesting to consider the general case where the coupling between the heat release rate and the pressure is non-uniform. The coupling parameter β is now expressed as

$$\beta = \beta_0\left(1+\sum_{m=1}^{M} C_m\cos(m\theta)+D_m\sin(m\theta)\right). \tag{12}$$

The RHS of eqn (2) is now

$$S_1 = \frac{1}{\pi}\int_0^{2\pi}\cos(n\theta)\beta_0\left(1+\sum_{m=1}^{M} C_m\cos(m\theta)+D_m\sin(m\theta)\right)\big(\dot{\eta}_1\cos(n\theta)+\dot{\eta}_2\sin(n\theta)\big)\,d\theta \tag{13}$$

Expanding this expression and performing the azimuthal integrations[3] yields

$$S_1 = \beta_0\dot{\eta}_1\left(1+\frac{C_{2n}}{2}\right)+\beta_0\dot{\eta}_2\frac{D_{2n}}{2} \tag{14}$$

[3]Making use of the following integral relationships

$$\int_0^{2\pi}\cos^2(n\theta)\cos(m\theta) = \begin{cases} 0 \text{ when } m\neq 2n \\ \frac{\pi}{2} \text{ when } m=2n \end{cases} \qquad \int_0^{2\pi}\cos(n\theta)\sin(n\theta)\sin(m\theta) = \begin{cases} 0 \text{ when } m\neq 2n \\ \frac{\pi}{2} \text{ when } m=2n \end{cases}$$

$$\int_0^{2\pi}\cos^2(n\theta)\sin(m\theta) = 0 \;\; \forall\, m \qquad \int_0^{2\pi}\cos(n\theta)\sin(n\theta)\cos(m\theta) = 0 \;\; \forall\, m$$

Applying the same procedure to the RHS of eqn (3) gives

$$S_2 = \beta_0 \dot{\eta}_2 \left(1 - \frac{C_{2n}}{2}\right) + \beta_0 \dot{\eta}_1 \frac{D_{2n}}{2} \tag{15}$$

Since the azimuthal origin can be defined arbitrarily, it is chosen such as $D_{2n} = 0$. We proceed now with the integration over time as in Section 2.1, in order to obtain the modal amplitude equations of the general case:

$$\dot{A} = \frac{1}{2}\left(\beta_0\left(1 + \frac{C_{2n}}{2}\right) - \alpha\right) A - \frac{k}{32}(9A^2 + 3B^2)A \tag{16}$$

$$\dot{B} = \frac{1}{2}\left(\beta_0\left(1 - \frac{C_{2n}}{2}\right) - \alpha\right) B - \frac{k}{32}(9B^2 + 3A^2)B \tag{17}$$

Calculation of the fixed points ($\dot{A} = \dot{B} = 0$) gives four types of solutions:

$$\begin{array}{lll} \text{(solution 1)} & A = 0, & B = 0 \\ \text{(solution 2)} & A = 0 & B = \frac{4}{3}\sqrt{\frac{\beta_0(1-C_{2n}/2)-\alpha}{k}}, \\ \text{(solution 3)} & A = \frac{4}{3}\sqrt{\frac{\beta_0(1+C_{2n}/2)-\alpha}{k}} & B = 0, \\ \text{(solution 4)} & A = 2\sqrt{\frac{\beta_0(1+C_{2n})-\alpha}{3k}}, & B = 2\sqrt{\frac{\beta_0(1-C_{2n})-\alpha}{3k}} \end{array} \tag{18}$$

Calculation of the eigenvalues of the coupled system (eqns (16) and (17)) successively linearised around the fixed points given in eqn (18) provides the stability nature of each of these limit cycles. The eigenvalues of this system are:

$$\begin{array}{lll} \text{(solution 1)} & \lambda_1 = \frac{1}{2}(\beta_0(1 + C_{2n}/2) - \alpha), & \lambda_2 = \frac{1}{2}(\beta_0(1 - C_{2n}/2) - \alpha) \\ \text{(solution 2)} & \lambda_1 = \frac{1}{3}(\beta_0(1 + C_{2n}) - \alpha), & \lambda_2 = \alpha - \beta_0(1 - C_{2n}/2) \\ \text{(solution 3)} & \lambda_1 = \alpha - \beta_0(1 + C_{2n}/2), & \lambda_2 = \frac{1}{3}(\beta_0(1 - C_{2n}) - \alpha) \\ \text{(solution 4)} & \lambda_1 = \frac{3}{4}(\alpha - \beta_0) + \frac{1}{4}\sqrt{(\alpha-\beta)^2 + 8\beta_0^2 C_{2n}^2}, & \lambda_2 = \frac{3}{4}(\alpha - \beta_0) - \frac{1}{4}\sqrt{(\alpha-\beta)^2 + 8\beta_0^2 C_{2n}^2} \end{array} \tag{19}$$

First, it can be noted that if the distribution is defined such that $C_{2n} = 0$, the stability of the different limit cycles is identical to the case of a uniform distribution of the sources driven by the "pressure/heat release" coupling. However, it can be seen that if $C_{2n} \neq 0$, the limit cycle amplitudes and stability can noticeably differ from the uniform distribution case.

It is thus interesting to plot the eigenvalues of the system as function of C_{2n} for a linearly unstable case operating on the n^{th} azimuthal mode, for which $\beta_0 > \alpha$. This is presented in Fig. 1. The 4 diagrams provide the stability nature of the 4 different types of fixed points given in eqn (18). Solution 1, which is the non-oscillating equilibrium, always feature at least one unstable eigenvalue and is either a repeller or a saddle point depending on the coefficient C_{2n} of the spatial distribution (in agreement with the linearly unstable assumption $\beta_0 > \alpha$). Solution 2 is also an unstable fixed point for any C_{2n}. One can note that solution 2 and 3 are not symmetric, except when $C_{2n} = 0$. This is due to the fact that we have chosen the origin such as $D_{2n} = 0$.

However, solution 3 and 4 can have stable limit cycles depending on the C_{2n} value. This is observed when the two eigenvalues λ_1 and λ_2 are both negative, and these regions are shaded on the lower subfigures. The eigenvalues of these two fixed point types share a common C_{2n} threshold (vertical dashed line) for which the stability nature of the system is switching from one type to the other type of limit cycle. This threshold $(\beta_0 - \alpha)/\beta_0$ can be deduced from eqns (19).

When $C_{2n} = 0$, the stable fixed point is given by solution 4, which features 2 negative eigenvalues. This solution corresponds to a rotating mode in the annular combustion chamber, since the azimuthal modal amplitudes A and B are identical. When $0 < C_{2n} < (\beta_0 - \alpha)/\beta_0$, solution 4 is still an attractor and defines the nature of the limit cycle. The modal amplitudes A and B are now different, which corresponds to a situation where the limit cycle is a combination of standing and spinning waves. For $C_{2n} > (\beta_0 - \alpha)/\beta_0$, solution 4 is now unstable, and solution 3, which was for the previous range a saddle

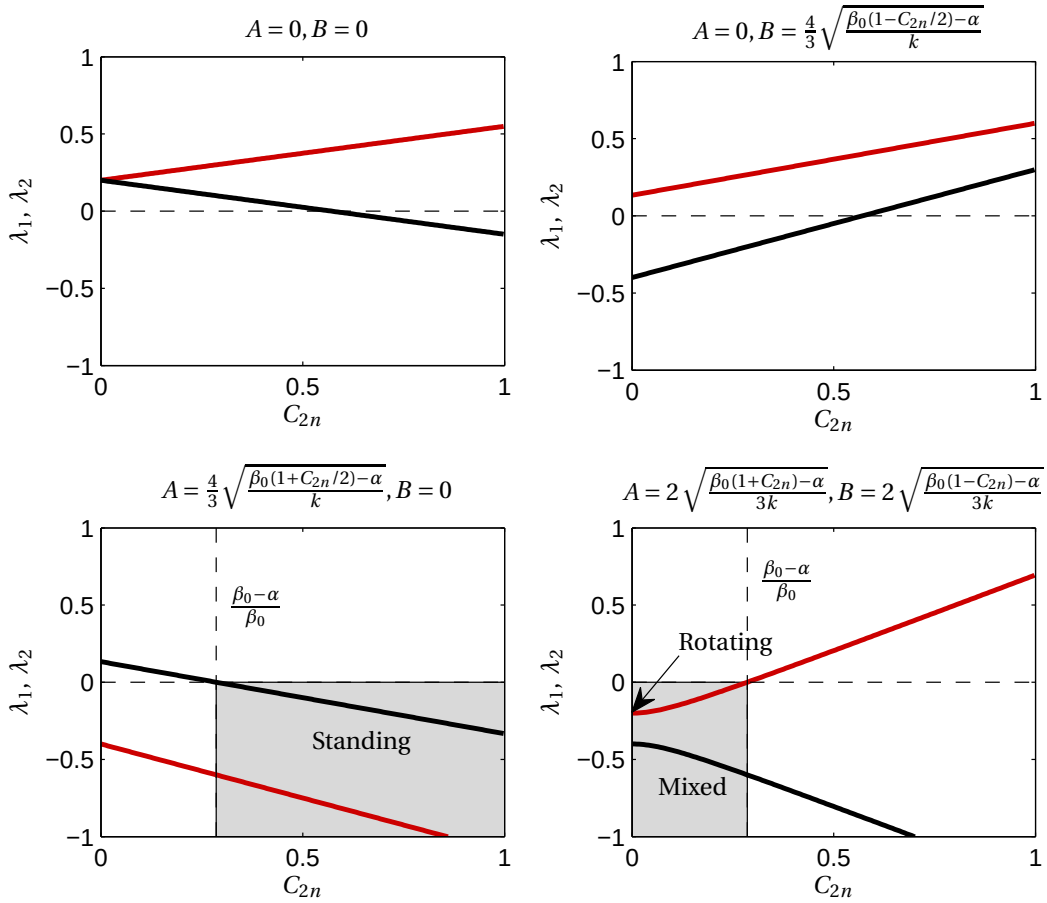

Figure 1: Eigenvalues of the fixed points defined in eqn (18) plotted as function of C_{2n}. The presented curves are calculated for $\beta_0 = 1.4$ and $\alpha = 1$. Each subfigure corresponds to one of the 4 types of solutions. If both λ_1 and λ_2 are positive (resp. < 0) the corresponding fixed point is unstable (resp. stable). The vertical dashed line corresponds to a threshold for C_{2n} where the stability nature of the system is changing (as described in the text).

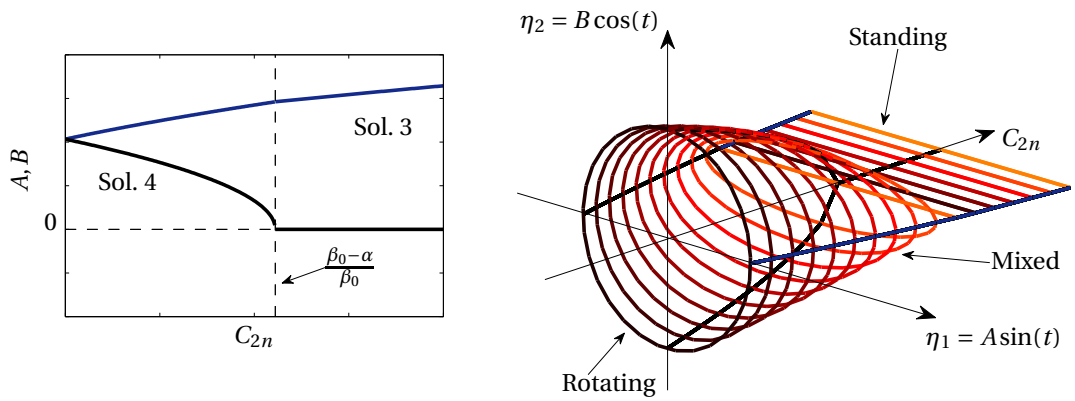

Figure 2: Left: Stable fixed points defined in eqn (18) plotted as function of C_{2n}. The presented curves are calculated for $\beta_0 = 1.4$, $\alpha = 1$ and $k = 0.2$. Right: Corresponding limit cycle amplitudes η_1 and η_2 for different C_{2n}.

point, becomes an attractor and defines the limit cycle nature: a standing wave pattern is established since $B = 0$.
In conclusion, if the $2n$ order contribution in the spatial distribution of the source term is larger than the threshold $(\beta_0 - \alpha)/\beta_0$, a standing mode operates in the chamber. If this contribution is decreased, by modifying the angular distribution, down to the threshold, the limit cycle switches from a standing to a mixed "standing/spinning" mode. When the $2n$ order angular contribution vanishes, the fixed point becomes a purely rotating n^{th} azimuthal mode. The bifurcation diagram is presented in Fig. 2.

3 Simulations

The theoretical results derived in the previous section are compared to simulations performed with the thermoacoustic network tool *Ta*3 developed in-house. The principle of this modular acoustic network is explained in detail in [8–10]. Therein, comparisons of *Ta*3 simulations with engine data are also shown demonstrating the strong capabilities of this tool to efficiently reproduce thermoacoustic coupling in heavy duty gas turbines. It consists of a hybrid approach: numerical, experimental and analytical techniques are combined to describe the system.
The modules are defined in the Matlab/Simulink environment. The state-space representation of the acoustic propagation through complex 3-dimensional geometries is obtained by expanding the acoustic variables on a modal basis, which is either obtained analytically when the configuration considered is simple, or by using finite element calculations. The flame transfer functions (FTF) and source terms are incorporated by fitting state space models to measured data. The state-space network approach allows either for time domain simulations, including non-linearities or frequency domain calculations. An eigenvalue analysis can thus be performed, which is straightforward due to the state-space formulation.
By using this causal representation of the combustor – annular plenum and combustion chamber connected via the burners – temporal simulations are performed (5^{th} order Dormand-Prince time integration) to provide the acoustic pressure in the chamber at the burners' azimuthal locations. It is possible to assign any FTF to the individual burners due to the modularity of the tool, and thus to investigate the influence of azimuthal FTF distributions on pulsations.
In what follows, results obtained with *Ta*3 are compared to the analytical derivations developed in the previous section. The influence of the distribution of different FTFs is investigated by considering 3 configurations. These configurations differ by the fact that one part of the burners features flames having an acoustic response given by FTF_1; the remaining being dynamically characterized by FTF_2. The azimuthal distributions for FTF_1 and FTF_2 burners are given in Fig. 3. FTF_1 is assigned to 6 out of 24

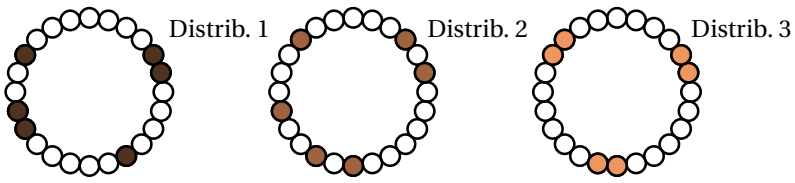

Figure 3: Angular distribution of the 6 flames characterized by FTF_1 (colored circles) and the 18 remaining ones whose dynamics are defined by FTF_2 (white circles).

burners; the angular distribution differs for the 3 configurations. The transfer functions FTF_1 and FTF_2, which are implemented in the thermoacoustic network, are presented in Fig. 4. The circles correspond to the measured data, while the solid lines are the FTF gains and phases of the best fit state-space model (state-dimension: order 8).
These transfer function combinations were chosen because they induce a linearly unstable 2^{nd} order azimuthal mode at frequency f_2 for the given acoustic losses. Time domain simulations for the different cases (distributions 1, 2 and 3) provide pressure signals at the flame locations. The normalized power

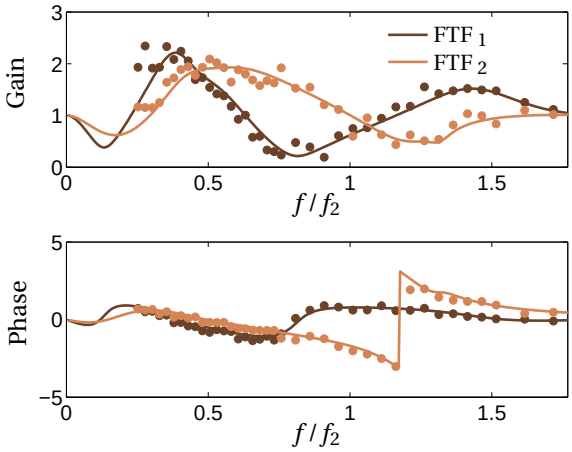

Figure 4: Flame transfer functions $\mathrm{FTF}_{1,2}$ implemented in the network for. The FTF definition used here links the upstream velocity perturbation at the burner outlet to the one downstream of the flame: $u_d = \mathrm{FTF}_{1,2} u_u$. circles: measurements; solid line: identified model.

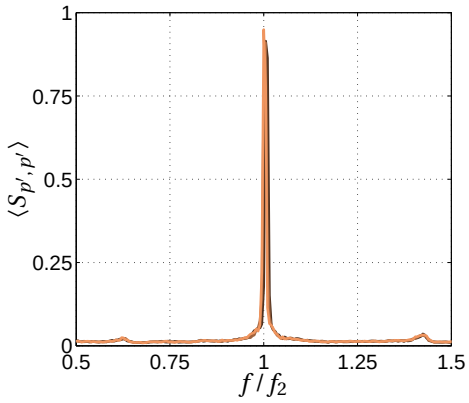

Figure 5: Normalized power spectral density (PSD) of the fluctuating pressure p' for the 3 distributions shown in Fig. 3. The quantity plotted is the mean PSD calculated from the 24 output pressure signals (one per flame).

spectral density of the acoustic pressure averaged over the 24 burners is given in Fig. 5. It is calculated from temporal data of the system operating at the limit cycle. A snapshot of the instantaneous fluctuating pressure field is given in Fig. 6 for the limit cycle obtained with distribution 1.

For the chosen FTF combinations, the system exhibits a linearly unstable 2$^{\mathrm{nd}}$ order azimuthal eigenmode, i.e., $n = 2$. According to the theoretical results obtained in Sec. 2, the component $C_{2n} = C_4$ of the angular distribution will define the "standing/spinning" nature of the limit cycle. Distribution 1 has the highest 4$^{\mathrm{th}}$ order azimuthal component (and thus the highest C_4 value for the adequate azimuthal origin), while it is vanishing for distribution 3; the value for distribution 2 is in between. Equations (16) and (17) yield a degenerate eigenvalue $\lambda_1 = \lambda_2 = (\beta_0 - \alpha)/2$ for distribution 3 since C_4 is vanishing. According to the model, this eigenvalue should split for distributions 1 and 2 which feature non-zero 4$^{\mathrm{th}}$ order azimuthal contributions:

$$\lambda_1 = \frac{1}{2}\left(\beta_0\left(1+\frac{C_4}{2}\right)-\alpha\right) \quad \text{and} \quad \lambda_2 = \frac{1}{2}\left(\beta_0\left(1-\frac{C_4}{2}\right)-\alpha\right).$$

In particular, the eigenvalue should split in a symmetric fashion around the degenerate one with a larger divergence for distribution 1 which has the largest C_4 value. The poles of the thermoacoustic network model corresponding to the second azimuthal mode at frequency f_2 are shown in Fig. 7.

As expected it can be seen that the eigenvalues of distribution 3 nearly coincide and are thus quasi-degenerate. For distributions 1 and 2, the imaginary part of these eigenvalues diverge up and down nearly symmetrically from the quasi-degenerate poles of distribution 3. The C_4 value for distribution 1 is largest. In agreement with the theory, the distance between the corresponding eigenvalues is also largest.

For each configuration, the cross spectral densities (CSD) of the pressure time traces between the reference signal p'_{ref} (azimuthal location where the PSD peak at f_2 is the highest) and each of the 23 remaining p'_j are calculated. Amplitude and phase of these CSDs at the peak frequency f_2 are shown in Fig. 8a. In the case of distribution 3, the phase angle linearly increases with the azimuthal coordinate and the amplitude of the CSD is nearly constant. This behavior indicates that the limit cycle is a rotating mode. This is in agreement with the theoretical model which states that vanishing C_4 component result in a rotating mode, which is the only possible stable limit cycle (solution 3 in Fig. 1).

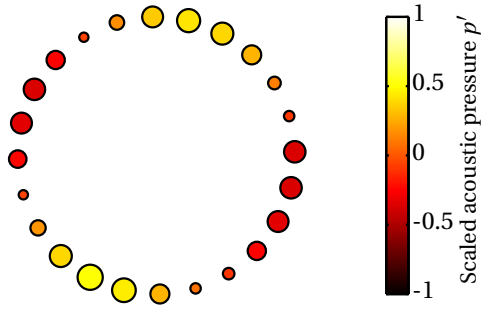

Figure 6: Instantaneous snapshot of the acoustic pressure field in the combustion chamber taken from the 24 output pressure signals at burner locations, when the limit cycle of the time domain simulation has been reached (dist. 1). The size of the circles is proportional to the acoustic pressure amplitude. The color indicate whether the fluctuation is positive or negative.

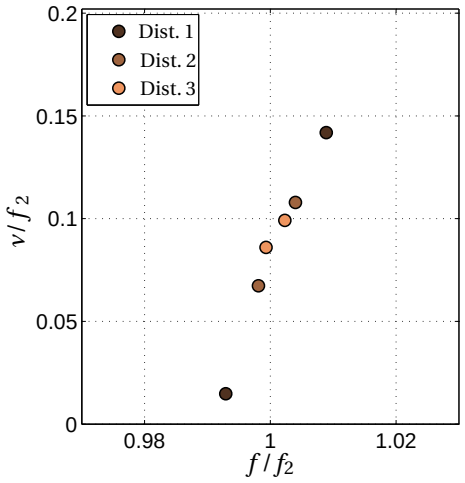

Figure 7: Eigenvalues of 2nd azimuthal mode. The normalized linear growth rates (imaginary part of the eigenvalues) are plotted as function of the normalized frequency (real part of the eigenvalues).

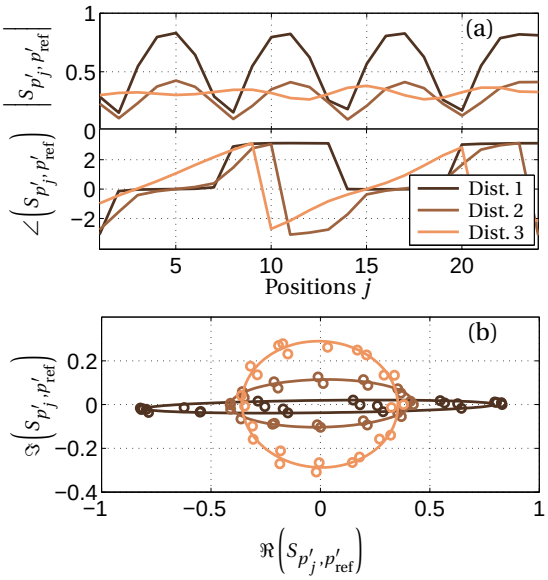

Figure 8: (a) Cross Spectral Density at frequency f_2 between the acoustic pressure p'_j at the different azimuthal locations j, and the reference signal p'_{ref} (featuring the highest peak amplitude). (b) Evolution of the CSD in the complex plane.

For distribution 1, the pressure signals are either in or out of phase with the reference acoustic pressure. This observation allows to conclude that for this distribution, the limit cycle is a standing mode for which the nodes are located at phase jumps of π. According to the model, large C_4 contributions in the azimuthal distribution cause a stable fixed point to be a standing mode (solution 4 in Fig. 1). This is also observed from the network simulations.
Distribution 2 is an intermediate situation where the phase and gain of the CSD indicate a combination of standing and spinning oscillation. It corresponds to the solution type 3 of the theoretical model, for which C_4 is not large enough to allow for an purely standing mode.
TIn Fig. 8b, these CSDs are plotted in the complex plane: circular, elliptical and linear trajectories correspond to rotating, mixed "spinning/standing" and purely standing modes, respectively.

The previous simulation results closely follow the theoretical predictions regarding the nature of the different limit cycles as a function of the system asymmetries. They have been obtained with an advanced thermoacoustic network model of a gas turbine, including modal descriptions for complex geometries that are obtained from FEM analyses, burner and flame state-space models fitted on measured data (see Fig. 4), and a non-linear amplitude saturation adjusted to reproduce engine data. Nevertheless one of the parameters that has been used here is unrealistically small: the source term. Since the theoretical model is derived from a small perturbation analysis, it has first been attempted to check the accuracy of these predictions with a weak source resulting in excellent agreement. The implementation of a realistic frequency dependent source term (state-space model fitted on measured data of the non-coherent dynamics of the flame) in the model induces a different type of limit cycle as shown in Figs. 9 and 10. In case of small perturbations, distribution 1 results in a standing mode limit cycle, whereas a realistic

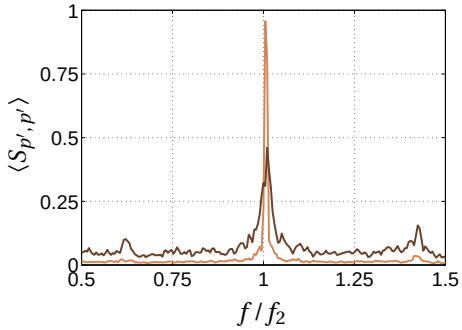

Figure 9: Limit cycle PSDs for distribution 1. The light-coloured curve corresponds to a simulation with weak source term whereas the dark one to a realistic non-coherent source (model fitted to measured data).

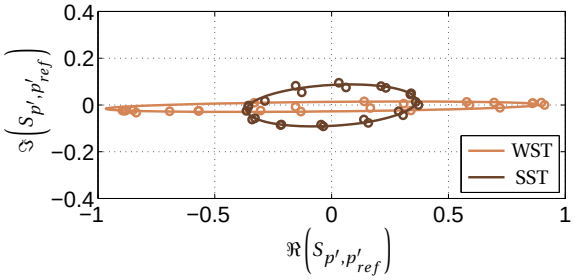

Figure 10: Evolution of the limit cycle CSDs in the complex plane for distribution 1: weak (unrealistic) and strong (measured) source term (light-coloured and dark curves, respectively).

source term in the time domain simulation causes a mixed type "spinning/standing" oscillation, which is actually observed in practical configurations. Nevertheless, the amplitude of the source term does not change the stability nature of the system, and the eigenvalues, which depend on the azimuthal FTF distribution, remain the same. It is therefore important to make use of the theoretical results presented in this study to set a favorable distribution in order to efficiently attenuate pulsations in practical systems.

4 Influence of the distribution of acoustic losses

According to a spatial distribution of FTFs, also a distribution of loss terms has a significant influence on system stability. Mathematically, this is expressed by assigning a spatial distribution to the loss term α in eqns (2) and (3) similar to that defined for β in eqn (12). In a gas turbine, these loss terms correspond to some kind of damping device, e.g., a Helmholtz damper or a perforated liner. By imposing a distribution of α, only a constant, real-valued impedance for the acoustic loss term is accounted for. Clearly, this does not correctly represent the frequency dependent, complex-valued impedance of, e.g., a Helmholtz damper, being defined by a 2$^{\text{nd}}$ or higher order dynamic system. However, as will be shown below, the results obtained for the simplified approach are able to predict the correct trends for the real system – gas turbine with damping devices – as well.

As in the previous section, an annular-type combustion chamber is considered for which the 2$^{\text{nd}}$ azimuthal mode is unstable. First, the system behavior for six loss term distributions is calculated, which differ in the degree of symmetry; thus their C_{2n} value (see Tab. 1). The acoustic losses are positioned as such that the C_4 value is gradually decreased from distribution 1 to 6. Since we are considering the 2$^{\text{nd}}$ azimuthal mode, locating the loss terms in a "X"-like pattern has the highest C_4 value. A network simulation of an annular gas turbine equipped with damping devices was conducted to study the influence

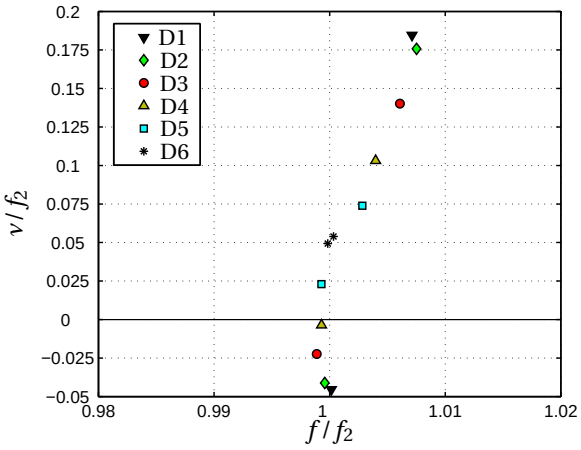

Figure 11: Growth rate versus frequency for different spatial distributions of the acoustic losses. The system considered here is a gas turbine equipped with dampers.

Distribution	1	2	3	4	5	6
C_4	20.3	19.0	14.8	10.1	5.6	0

Table 1: Values of C_4 for the different configurations.

of the loss term distribution in a real system. The gas turbine in this model is equipped with Helmholtz dampers. Figure 11 shows the growth rates of the 2$^{\text{nd}}$ azimuthal mode for the six cases. The horizontal solid line represents the stability border with a growth rate of 0. Poles below this line are stable, those above have a positive growth rate. The graph clearly shows the influence of the distribution of acoustic losses on the growth rates of the modes. It can be seen that the higher the C_{2n} value (cf. to Tab. 1), the larger is the maximum growth rate of the respective pole pair respresenting the 2$^{\text{nd}}$ azimuthal mode and the larger is the difference in growth rates of one pair. The first four distributions exhbit one mode that is stable whereas for cases 5 and 6 both are unstable. For distribution 6 ($C_{2n} = 0, *$), both poles have almost the same growth rate and frequency; they are nearly degenerate. The maximum growth rate for this distribution is smallest, i.e., the damping performance is highest. The mode considered has 4 nodes all laying $\pi/4$ apart from each other. In case of dampers, the pressure fluctuation at the damper location is minimzed. Thus, the condition for which the mode fulfills the prescribed "azimuthal boundary condition" best is the one for which it is merely turned inside the combustion chamber as such that its nodes coincide with the locations of the dampers. In this case, however, the damping efficiency is minimum. From the simplified theory, the split of the poles is calculated to be symmetric (cf. to eqns (16) and (17)), i.e., the value by which one of the mode's growth rate is increased corresponds to that by which the other is decrease. Similar observations based on symmetry considerations were also observed by Moeck and Paschereit [5]. They considered an asymmetry in the heat release model of an annular Rijke tube. In the system considered here, this seems only to be correct if both modes are unstable or marginally stable (distributions 1-3). Decreasing the homogenity (4-6), the growth rate of the unstable mode is increased more than that of the stable one is decreased.

Despite the simplifications made, the model is able to predict the correct trends of the more complex system represented by a gas turbine equipped with dampers. However, from this it cannot be deduced that it will be the case for all applications in which real damping devices are used. The fact that the performance of different damper distributions in a gas turbine can be predicted is a very important observation and will be investigated further on. The objective is to derive rules for which the system behavior is transferable and where the limits are.

5 Conclusion

In this study, the dynamic nature of azimuthal modes resulting from thermoacoustic interactions in annular combustion chambers is investigated. In order to identify the key parameters that are responsible for the standing or spinning mode nature, standard methods of dynamic system theory are applied. A third order non-linearity is introduced into the governing equations to model the heat release saturation of self-excited flames. A system of coupled differential equations describing the dynamics of the modal amplitude is obtained. This allows to derive simple analytical statements. The system dynamics are investigated by including asymmetries in the azimuthal distribution of the flame transfer function as well as damping devices. It is shown that, in the case of an unstable n^{th} azimuthal mode, the $2n$ component of the Fourier expansion of the azimuthal FTF distribution can be used as a bifurcation parameter. If this parameter is vanishing, the n^{th} azimuthal mode is rotating and degenerate eigenvalues are associated to this mode. If it exceeds a defined threshold, a standing mode is established in the annular chamber. In between, a mixed "spinning/standing" nature is predicted by the model. This is confirmed by advanced thermoacoustic network simulations for a practical configuration.

References

[1] Izhak Bucher. Estimating the ratio between travelling and standing vibration waves under non-stationary conditions. *J. Sound & Vib.*, 270:341–359, 2004.

[2] Y. Huang and V. Yang. Dynamics and stability of lean-premixed swirl-stabilized combustion. *Prog. Energy Combust. Sci.*, 35:293–364, 2009.

[3] W. Krebs, P. Flohr, B. Prade, and S. Hoffmann. Thermoacoustic stability chart for high intensity gas turbine combustion system. *Combust. Sci. Technol.*, 174(7):99–128, 2002.

[4] T. C. Lieuwen and V. Yang. *Combustion instabilities in gas turbines, operational experience, fundamental mechanisms, and modeling.* American Institute of aeronautics and astronautics, Inc., 2005.

[5] J. P. Moeck and C. O. Paschereit. Modeling thermoacoustic instabilities in an annular rijke tube: Asymmetries and standing and spinning modes. In *ICSV 16th Proceedings*, Krakòw, Poland, 2009.

[6] A. S. Morgans and S. R. Stow. Model-based control of combustion instabilities in annular combustors. *Combust. & Flame*, 150:380–399, 2007.

[7] S. Rea, S. James, C. Goy, and M. J. F. Colechin. On-line combustion monitoring on dry low nox industrial gas turbines. *Measurement Science and Technology*, 14(7):1123–1130, 2003.

[8] B. Schuermans. *Modeling and control of thermoacoustic instabilities.* Ph. D. thesis nr. 2800, EPFL, http://library.ep.ch/theses/?nr=2800, Lausanne, Switzerland, 2003.

[9] B. Schuermans, F. Guethe, D. Pennel, D. Guyot, and C. O. Paschereit. Thermoacoustic modeling of a gas turbine using transfer functions measured at full engine pressure. In *Proceedings of the ASME Turbo Expo 2009*, Orlando, USA, 2009.

[10] B. Schuermans, C. O. Paschereit, and P. Monkewitz. Non-linear combustion instabilities in annular gas turbine combustors. In *AIAA paper 2006-0549, 44th AIAA Aerospace sciences meeting and exhibit*, Reno, Nevada, 2006.

[11] J. R. Seume, N. Vortmeyer, W. Krause, J. Hermann, C.-C. Hantschk, P. Zangl, S. Gleis, D. Vortmeyer, and A. Orthmann. Application of active combustion instability control to a heavy duty gas turbine. *Journal of Engineering for Gas Turbines and Power*, 120(4):721–726, 1998.

[12] G. Staffelbach, L. Y. M. Gicquel, G. Boudier, and T. Poinsot. Large eddy simulation of self excited azimuthal modes in annular combustors. *Proc. Combust. Inst.*, 32:2909–2916, 2009.